# High strain rate superplasticity in an Al–Mg–Sc–Zr alloy subjected to simple thermomechanical processing

R. Kaibyshev [a], E. Avtokratova [a,*], A. Apollonov [a], R. Davies [b]

[a] *Institute for Metals Superplasticity Problems, Khalturina 39, Ufa, 450001, Russia*
[b] *Pacific Northwest National Laboratory, Richland, WA 99352, USA*

**Abstract**

Superior superplastic ductility of 2300% was achieved at 520 °C and $\dot{\varepsilon} = 5.6 \times 10^{-2}\ s^{-1}$ in an Al–5%Mg–0.2%Sc alloy produced by traditional chill casting followed by cold rolling with a total reduction of 80%.

*Keywords:* Superplasticity; Thermomechanical processing; Aluminum alloy; Mechanical properties

## 1. Introduction

The superplastic blow forming (SPF) manufacturing process is used for the fabrication of low-volume sheet metal components that have a complex shape [1]. There exist two main factors restricting the commercial application of SPF. First, sheets of superplastic aluminum alloys are relatively expensive due to the complex thermomechanical processing (TMP) typically necessary to make these materials superplastic [2]. Second, the forming times are generally in the range of 20–40 min for each component, due to the fact that these alloys exhibit superplasticity at a strain rate, $\dot{\varepsilon}$, of $\sim 10^{-3}\ s^{-1}$. As a result, the cost of the SPF production method can be prohibitive for high-volume production. The primary objective of this work is to report that a new aluminum alloy subjected to an inexpensive TMP procedure may exhibit a superplastic ductility at $\dot{\varepsilon} \sim 10^{-2}\ s^{-1}$, so that the forming time for each component will be in range of 1 min.

It was recently established that Al–Mg–Sc alloys subjected to large rolling reduction [3] or equal-channel angular extrusion (ECAE) [4–6], exhibit high strain rate superplasticity with highest ductilities of >1000%. Among the alloys of the Al–Mg–Sc system, the material with highest strength is the commercial Russian alloy Al–6%Mg–0.3%Sc, designated 1570 [7]. However, this material exhibits insufficient workability at ambient temperature [3,7], and extensive cracking results if this material is subjected to cold rolling with high reductions. It is very difficult to produce commercial-scale superplastic sheets from the 1570 alloy by traditional TMP [3]. Fortunately, a new version of the 1570 alloy, denoted here as 1570c Al, was very recently developed [8]. The 1570c Al alloy exhibits enhanced workability at room temperature in comparison with traditional 1570 Al [4,6], which allows this material to undergo cold rolling without cracking. Notably the mechanical properties of the 1570c Al at room temperature are similar to those of AA2004 alloy after standard aging [1,8]. In addition, the 1570c Al is a non-heat treatable alloy, which greatly facilitates the fabrication of articles by SPF due to elimination of quench distortions.

## 2. Material and experimental procedure

The 1570c Al with a chemical composition of Al–5%Mg–0.18%Mn–0.2%Sc–0.08%Zr–0.002%Be (in weight %) was

* Corresponding author. Tel.: +7 3472 253856; fax: +7 3472 253759.
*E-mail addresses:* rustam@anrb.ru (R. Kaibyshev), lena@imsp.da.ru (E. Avtokratova).

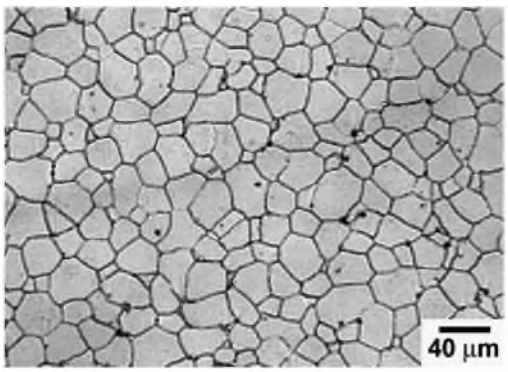


Fig. 1. Initial structure of the 1570c alloy after solution treatment.

cast into a steel mold to form an ingot with dimensions of $90 \times 220 \times 220\ mm^3$. The ingot was homogenized in air at 350 °C for 6 h. Next, each surface was scalped to remove ~10 mm. The ingot was cut into plates with dimensions of $10 \times 50 \times 70\ mm^3$. These plates were rolled at ambient temperature with a total reduction of 80% to the final thickness of ~2 mm. A six-high mill with internal rollers 65 mm in diameter and 250 mm in length was used. Notably, no significant cracking took place on the lateral surfaces of the rolled sheets.

Tensile specimens with a 6 mm gauge length and 3 mm gauge width were machined from the final sheet; the gauge lengths were parallel to the rolling direction. Tensile tests were carried out in the temperature interval 475–550 °C at strain rates ranging from $2.8 \times 10^{-4}$ to $1.4 \times 10^{-1}\ s^{-1}$. Each sample was held at a testing temperature for about 5 min prior to applying load in order to reach a thermal equilibrium. The other details of mechanical testing and structural characterization were reported in previous works [3,9,10]. A JEOL JEM-2000EX electron microscope was used for the thin foil examinations. The density of lattice dislocation was calculated using the intercept method described in Ref. [10]. For surface examination, a specimen was mechanically polished, and line scratches were introduced using 1-μm diamond paste. Then the specimen was pulled at 520 °C and $\dot{\varepsilon} = 5.6 \times 10^{-2}\ s^{-1}$ up to a true strain, $\varepsilon$, of ~0.4. The offset or rotations of the marker lines were recorded by a JSM-6400 scanning electron microscope (SEM). Misorientations of low angle (LAGB) and high

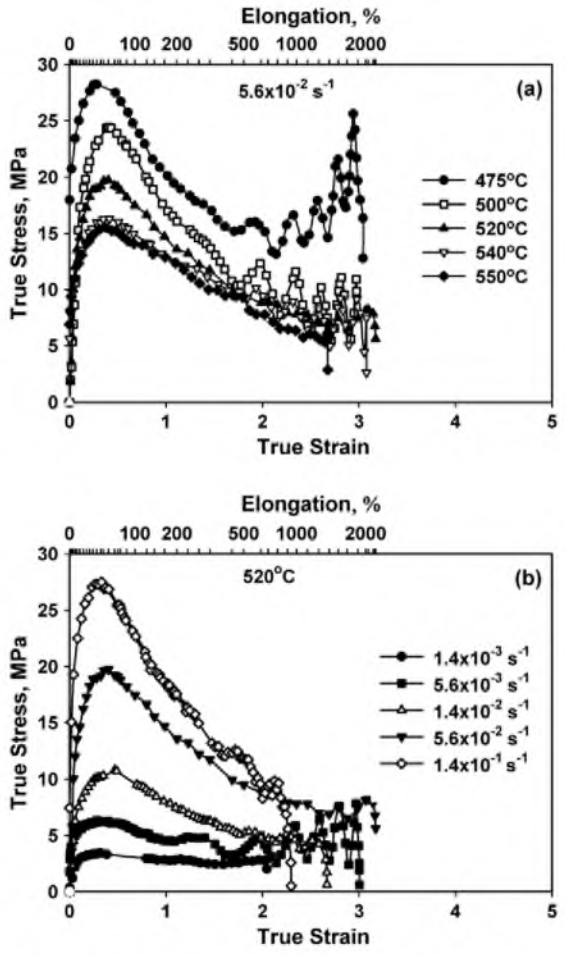


Fig. 2. Typical true stress–true strain curves of the 1570c alloy: (a) the temperature dependence, (b) the strain rate dependence.

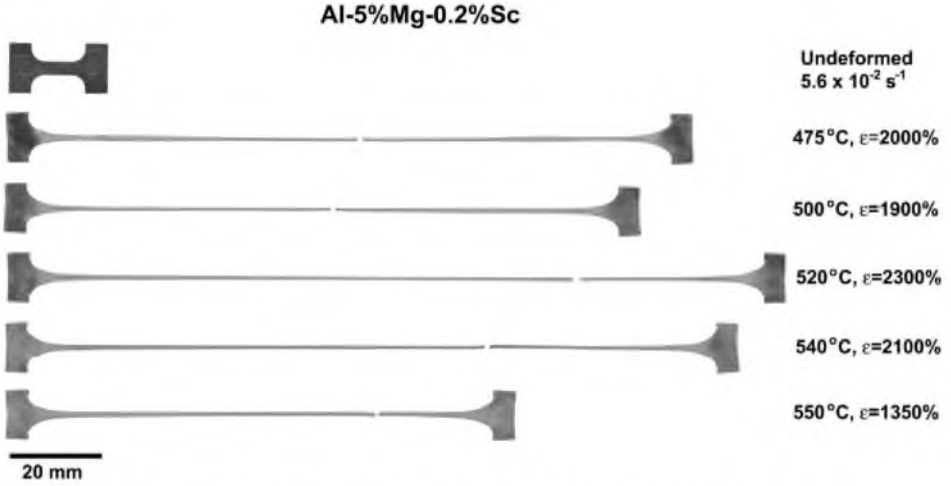


Fig. 3. Shadowgraphs of samples pulled to failure at a strain rate of $5.6 \times 10^{-2}\ s^{-1}$.

angle boundaries (HAGB) were studied by electron backscattering diffraction (EBSD) analysis using a JEOL JSM-840 A SEM equipped with an automated EBSD pattern collection system provided by Oxford Instruments. HAGBs ($\geqslant 15°$) and LAGBs (3–15°) are depicted in misorientation maps as dark and white lines, respectively.

## 3. Results

A typical microstructure of the 1570c Al after the solution treatment is shown in Fig. 1. The as-cast structure is very uniform; grains exhibit equiaxed shape, and their average size is ~24 μm (Fig. 1). Therefore, a greater refinement occurred under chill casting compared with the traditional version of the 1570 which has an average grain size of ~100 μm. The microstructure of the rolled 1570c alloy consists of high density tangled dislocations and cells of size ranging from 200 to 500 nm; which is similar to that reported for the traditional 1570 alloy [3].

Typical true stress–true strain ($\sigma$–$\varepsilon$) results are shown at an initial strain rate of $5.6\times10^{-2}\,s^{-1}$ and temperatures ranging from 475 to 550 °C in Fig. 2(a); and at a fixed temperature of 520 °C and strain rates ranging from $1.4\times10^{-3}$ to $1.4\times10^{-1}\,s^{-1}$ in Fig. 2(b). These figures show that extensive strain hardening takes place initially at all temperatures and $\dot{\varepsilon}\geqslant 5.6\times10^{-3}\,s^{-1}$ (tests were conducted at constant crosshead velocity). After reaching a maximum, the flow stress continuously decreases until failure. A well-defined peak in flow stress is observed at $\varepsilon\sim0.4$; at $\varepsilon\geqslant 2$, a stress oscillation appears. An increase in temperature or a decrease in strain rate results in decreasing peak stress and a reduction in strain softening. At 520 °C and $\dot{\varepsilon}=1.4\times10^{-3}\,s^{-1}$, steady-state flow is attained. Very uniform deformation within the gauge length occurs at all conditions, and pseudo-brittle fracture is observed (Fig. 3). As a result, the samples exhibit superior tensile ductility. In the temperature interval 475–540 °C at $\dot{\varepsilon}=5.6\times10^{-2}\,s^{-1}$, elongations are $\geqslant$1900% (Fig. 3).

Fig. 4(a) shows a plot of flow stress taken at $\varepsilon\sim0.4$. Strain rate dependencies of the coefficient of strain rate sensitivity, $m$, and elongation-to-failure, $\delta$, are also presented (Fig. 4(b) and (c)). The 1570c Al exhibits a sigmoidal relationship between the flow stress and strain rate with maximum strain rate sensitivity coefficient $m\sim0.5$ at $\dot{\varepsilon}\sim10^{-2}\,s^{-1}$; three well-known regions of superplastic deformation [2,9] can be identified in Fig. 4(a). The highest elongation-to-failure is observed at a higher strain rate of $5.6\times10^{-2}\,s^{-1}$. At 520 °C, very high $\delta$ values ($\geqslant$1300%) were found in the strain rate range $5.6\times10^{-3}\,s^{-1}$ to $5.6\times10^{-2}\,s^{-1}$. Thus, the 1570c alloy exhibits superior ductility at the relatively high strain rate of $\dot{\varepsilon}\sim10^{-2}\,s^{-1}$.

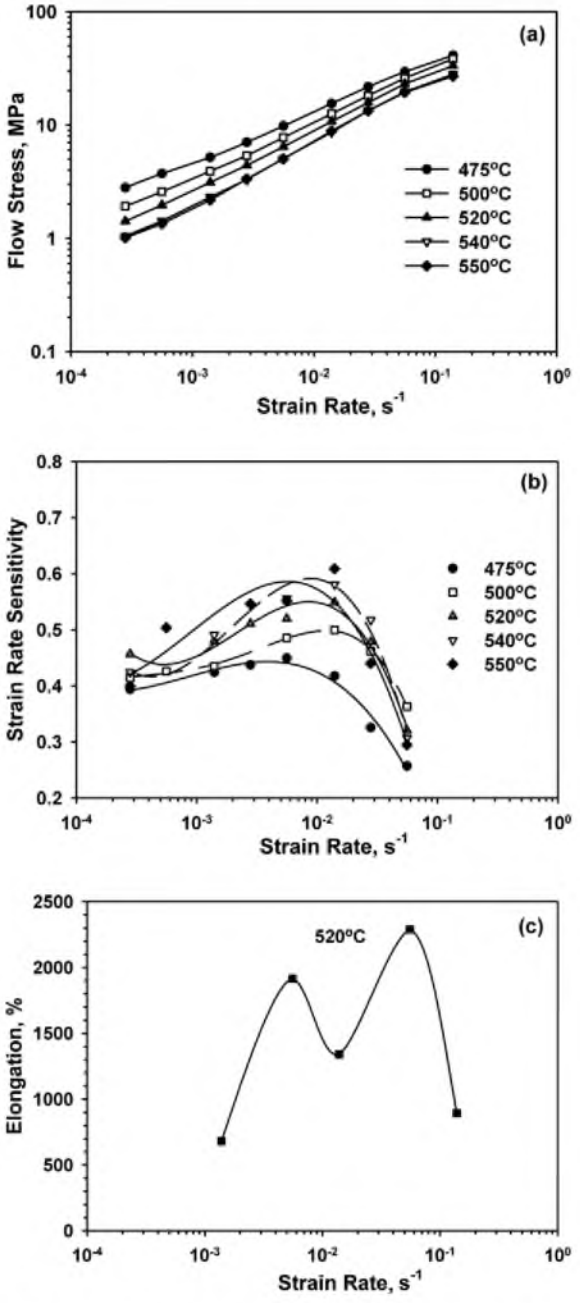


Fig. 4. The variation of flow stress: (a) strain rate sensitivity and (b) elongation to failure (c) with strain rate.

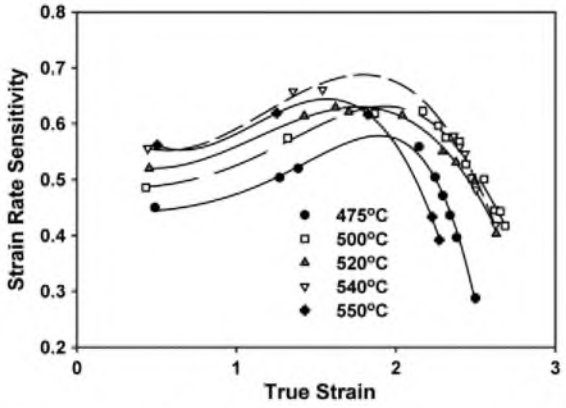


Fig. 5. The variation of strain rate sensitivity with true strain at strain rate of $5.6\times10^{-2}\,s^{-1}$.

Fig. 5 shows variations of the coefficient of strain rate sensitivity with strain. This figure shows that the $m$ value increases from ~0.5 to ~0.6 with increasing strain up to $\varepsilon \leqslant 1.8$ and tends to drop under further strain. However, at all temperatures except 475 °C, the $m$ value remains $\geqslant 0.35$ even at very high strains.

The microstructure evolution of the 1570c alloy was examined under both static and dynamic conditions in grip and gauge sections. A partially recrystallized structure evolves during annealing of the material (Fig. 6(a) and (b)). An average density of dislocation $\rho \sim 5 \times 10^{12}\ \mathrm{m}^{-2}$ was observed within interiors of recrystallized grains. Mixed arrays of LAGBs and HAGBs are formed within interiors of initial grains (Fig. 6(a)) under static annealing. Crystallites bounded partly by LAGBs and partly by HAGBs dominate. The formation of true grains entirely outlined by HAGBs is mainly observed near old boundaries. Their fraction is about 30%.

Superplastic deformation leads to complete transformation of LAGBs into HAGBs (Fig. 7) due to the occurrence of continuous dynamic recrystallization [3]. The population of HAGBs attains 96%. After superplastic deformation with $\varepsilon \sim 3$. It appears that all mobile lattice dislocations are adsorbed by HAGBs or trapped by LAGBs resulting in their eventual transformation into HAGBs during superplastic deformation [10], and no formation of new LAGBs takes place. At 520 °C and $\dot{\varepsilon} = 5.6 \times 10^{-2}\ \mathrm{s}^{-1}$, a fully recrystallized structure is evolved (Fig. 7(a)). The misorientation distribution with average angle close to 40.7 (Fig. 7(b)) is essentially that predicted by Mackenzie [11]. This Mackenzie-like misorientation distribution usually associates with extensive grain boundary sliding (GBS), which results in random lattice rotations during superplastic deformation [12]. In the same time, the grains are highly elongated along tension direction (Fig. 7(a)). The grain aspect ratio (AR), defined as the ratio of the grain dimension in the longitudinal direction (~15 μm) to that in the transverse direction (~5 μm), is ~3. This value of AR is indicative of a significant contribution of intergranular dislocation glide to the total elongation.

The superplastic deformation induces cavitation (Fig. 8). Cavities having a jagged shape are formed in the present work. Their volume fraction attains a very high value (~16%) just before failure. The average sizes of voids in tension and transverse directions are ~92 μm and ~22 μm, respectively. Therefore, coarse voids evolve during testing and are elongated parallel to the tension axis

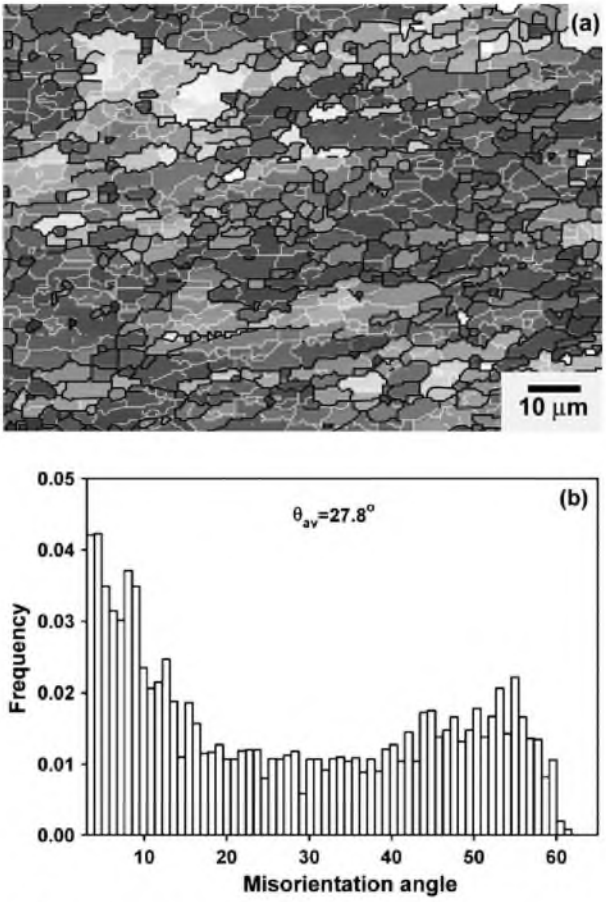


Fig. 6. Microstructure of the cold rolled 1570c Al after static annealing for 720 s at 520 °C in grip section: (a) typical EBSD map, (b) misorientation distribution.

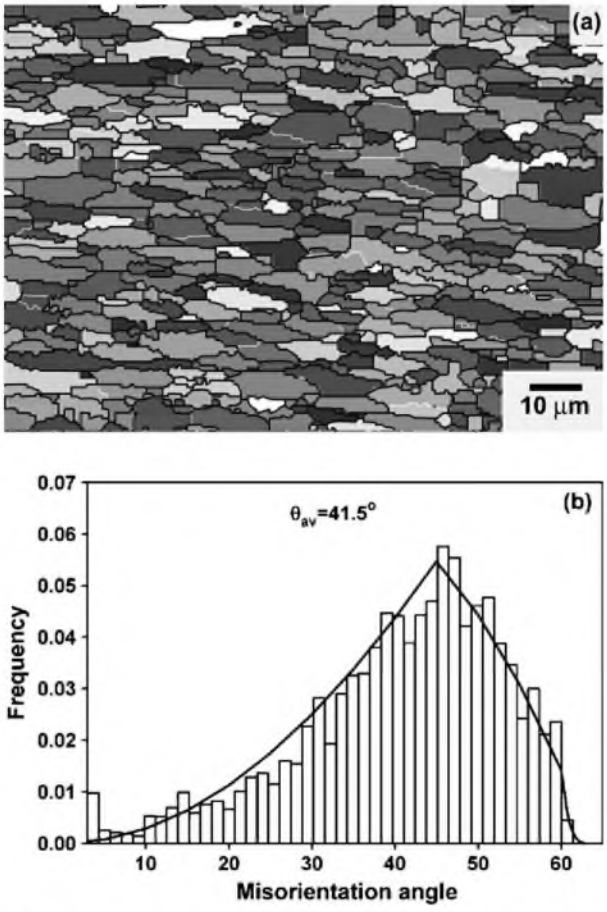


Fig. 7. Microstructure of the 1570c Al after superplastic deformation at 520 °C and $5.6 \times 10^{-2}\ \mathrm{s}^{-1}$ after $\varepsilon \sim 3.1$ in gauge section: (a) typical EBSD map, (b) misorientation distribution, solid line represents Mackenzie distribution [11].

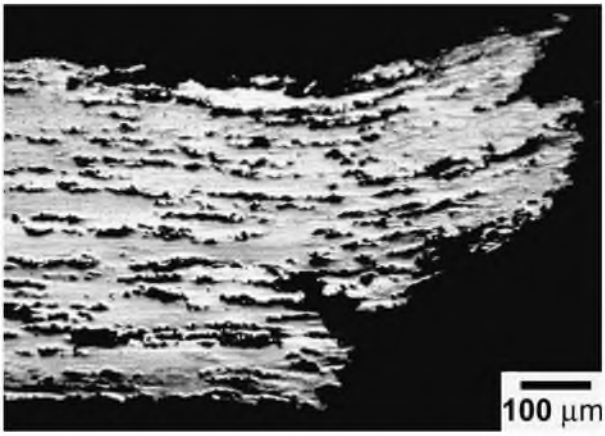


Fig. 8. Cross-sectional view of sample strained at 520 °C and $5.6 \times 10^{-2}\ s^{-1}$ up to $\varepsilon \sim 3.1$.

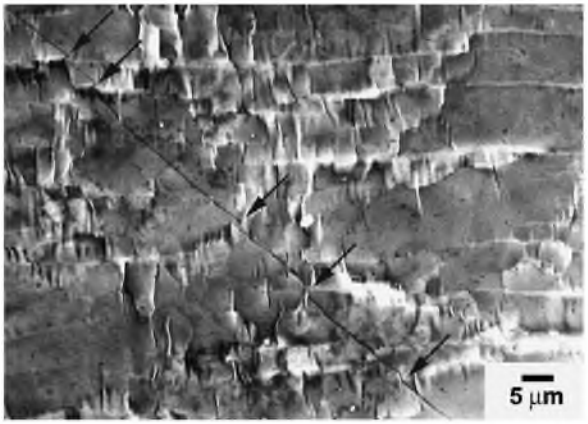


Fig. 9. Surface observation after superplastic deformation with $\varepsilon \sim 0.4$ at 520 °C and $5.6 \times 10^{-2}\ s^{-1}$. Arrows indicate the offsets of scratch lines.

with a cavity aspect ratio of ~4.5. Therefore, strain controlled cavity growth [2] takes place. It is apparent that very high porosity is associated with the fact that cavity interlinkage takes place only along the tension direction. As a result, very high elongations-to-failure can be achieved in the 1570c Al despite extensive cavitation. Pseudo-brittle fracture occurs due to crack propagation between void chains at an angle close to 45° to the tension axis. Interlinkage of the elliptical voids in the transverse direction appears to play an unimportant role in fracture.

Offsets of marker lines were observed both along initial boundaries and boundaries of recrystallized grains as well (Fig. 9). Therefore, sliding of initial grains gives a significant contribution to total elongation. The formation of new recrystallized grains increases the contribution of GBS. The textures are given in Fig. 10. It is seen that static annealing and superplastic deformation lead to texture randomization (Fig. 10). The formation of nearly random texture during superplastic deformation indicates operation of extensive GBS.

## 4. Discussion

A main feature of the 1570c alloy is a moderate grain size in the as-cast condition. A decreased fraction of $Al_3Sc$ dispersoids in the 1570c Al in comparison with 1570 Al due to decreased Sc content (0.2 instead of 0.35 wt.%) results in enhancement of superplastic properties. In the traditional 1570 Al, the nanoscale dispersoids exert a strong pinning effect on boundaries and no recrystallization occurs in the material under static annealing, which follows extensive rolling [3]. In contrast, the partially recrystallized grain structure is evolved under static annealing in the 1570c Al due to reduced boundary pinning pressure. As a result, GBS starts to occur at early stage of superplastic deformation in the 1570c Al (Fig. 9) along sufficient number of HAGBs. The extensive operation of GBS in the regions of crystallites bounded partly by LAGBs and partly by HAGBs requires increased flow stress [13] to provide the continuity between the sliding subgrain boundaries through the generation and absorption of lattice dislocations [14]. As a result, a well-defined peak stress takes place initially, and the transformation of LAGBs into HAGBs occurs at a high rate [13] providing grain refinement. An increase in the number of HAGBs, along which

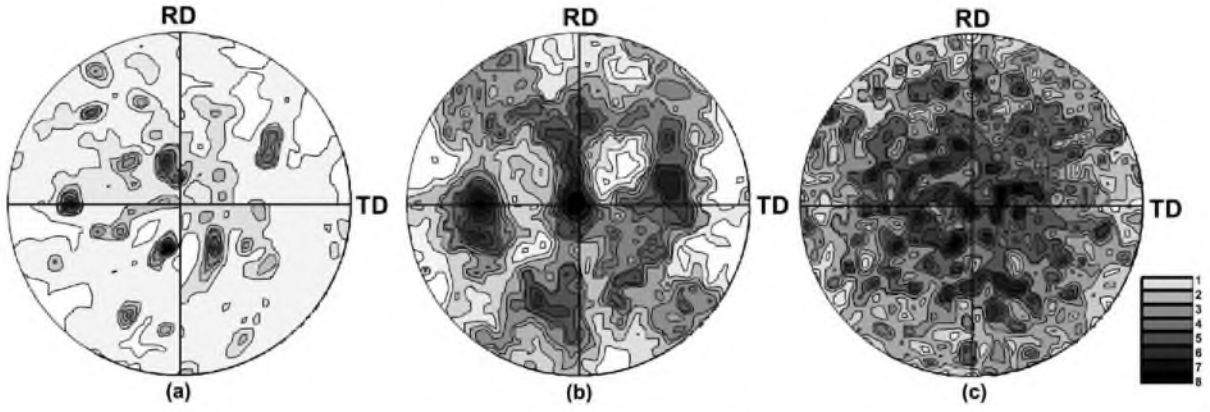


Fig. 10. {1 0 1} pole figures of the 1570c Al after (a) cold rolling, (b) annealing at 520 °C for 30 min, (c) superplastic deformation at 520 °C and $5.6 \times 10^{-2}\ s^{-1}$ up to $\varepsilon \sim 3.1$.

GBS occurs, results in the strain softening. No effect of strain on the coefficient of strain rate sensitivity was found, and, therefore, GBS is the dominant mechanism of superplastic deformation in the 1570c Al both with partially recrystallized structure and fully recrystallized structure providing random misorientation distribution and random texture.

The main feature of the microstructure in the 1570c alloy is the elongated shape of recrystallized grains. Sliding of elongated grains cannot be accommodated well, and stress concentration at triple junction may lead to extensive cavitation [2,15]. Voids were continuously nucleated, resulting in an increase in the cavity density with increasing strain. The linkage of cavities along tension direction at high strains leads to the formation of coarse voids having an elliptical shape.

Thus, superior superplastic ductility of 2300% was achieved in the new high-strength Al–Mg–Sc alloy at 520 °C and $\dot{\varepsilon} = 5.6 \times 10^{-2}\ s^{-1}$ by subjecting this material to intense cold rolling with a total reduction of 80%. A partially recrystallized structure evolved in the 1570c Al under static annealing before superplastic deformation. A fully recrystallized structure evolved during superplastic deformation.

## References


[1] Barnes AJ. Mater Sci Forum 2000;357–359:3.
[2] Pilling J, Ridley N. Superplasticity in crystalline solids. London: The Institute of Metals; 1989 [p. 214].
[3] Nieh TG, Hsiung LM, Wadsworth J, Kaibyshev R. Acta Mater 1998; 46:2789.
[4] Furukawa M, Utsunomiya A, Matsubara K, Horita Z, Langdon TG. Acta Mater 2001;49:3829.
[5] Komura S, Horita Z, Furukawa M, Nemoto M, Langdon TG. Metall Mater Trans A 2001;32:707.
[6] Horita Z, Furukawa M, Nemoto M, Barnes AJ, Langdon TG. Acta Mater 2000;48:3633.
[7] Filatov YuA, Yelagin VI, Zakharov VV. Mater Sci Eng A 2000;280: 97.
[8] Davydov VG, Filatov Yu, Lenczowski B, Yelagin V, Zakharov V. United States Patent #6,676,899, Eads Deutschland GmbH, 2004.
[9] Musin F, Kaibyshev R, Motohashi Y, Itoh G. Metall Mater Trans A 2004;35:2383.
[10] Kaibyshev R, Shipilova K, Musin F, Motohashi Y. Mater Sci Eng 2005;396:341.
[11] Mackenzie JK. Biometrika 1958;45:229.
[12] Eddahbi M, McNelley TR, Ruano OA. Metall Mater Trans A 2001; 32:1093.
[13] Yang X, Miura H, Sakai T. Mater Trans 2002;43:2400.
[14] Dougherty LM, Robertson IM, Vetrano JS. Acta Mater 2003;51: 4367.
[15] Ma ZY, Mishra RS. Acta Mater 2003;51:3551.